Chapter 29
Image Analysis: Intermediate Level Vision

Supplements

WILEY-VCH Verlag GmbH & Co. KGaA

Contents

Optical Digital Image Processing. Fundamentals and Applications. Edited by

ISBN: xx-xxx-x-xxx-xxxxx-x

A
Deformable Models: Mathematical Formulation (Discrete case)

A numerical solution to (Eq. 1.25) as given in Section 1.4.1, can be found by discretizing the equation and solving the discrete system iteratively. It is also possible to start directly from a discrete formulation of the energy functional in N nodes:

$$E^*_{tot} = \sum_{i=0}^{\mathrm{N}-1} E_{\mathrm{int}}(i) + E_{\mathrm{ext}}(i)\ , \tag{A.1}$$

which is the approach that is followed in this section.

We set $\mathbf{v}_i = (x_i, y_i) = (x(ih), y(ih))$ and approximate the derivatives $\mathbf{v}_s$ and $\mathbf{v}_{ss}$ by the finite differences[1)]:

$$\mathbf{v}_s = \frac{(\mathbf{v}_i - \mathbf{v}_{i-1})}{h} \text{ and } \mathbf{v}_{ss} = \frac{(\mathbf{v}_{i+1} - 2\mathbf{v}_i + \mathbf{v}_{i-1})}{h^2}\ . \tag{A.2}$$

Hence we obtain:

$$E_{\mathrm{int}}(i) \quad = \frac{w_1^i \left|\mathbf{v}_i - \mathbf{v}_{i-1}\right|^2}{2h^2} + \frac{w_2^i \left|\mathbf{v}_{i+1} - 2\mathbf{v}_i + \mathbf{v}_{i-1}\right|^2}{2h^4} \tag{A.3}$$

$$= \quad \frac{w_1^i((x_i - x_{i-1})^2 + (y_i - y_{i-1})^2)}{2h^2} \tag{A.4}$$

$$+ \quad \frac{w_2^i((x_{i-1} - 2x_i + x_{i+1})^2 + (y_{i-1} - 2y_i + y_{i+1})^2)}{2h^4}\ , \tag{A.5}$$

where $w_1^i = w_1(x_i, y_i)$ and $w_2^i = w_2(x_i, y_i)$.

For a closed contour i.e. $\mathbf{v}(0) = \mathbf{v}(\mathrm{N})$ the indexing $i-1$ should be understood as $(i-1)\mathrm{mod}(\mathrm{N})$ and $i+1$ as $(i+1)\mathrm{mod}(\mathrm{N})$. In the following, we just continue to use $i-1$ and $i+1$ to keep the notation simple. In order to reach a minimum the following conditions of stationarity should be fulfilled for all the nodes 0 to $\mathrm{N}-1$:

$$\frac{\partial E^*_{tot}}{\partial x_i} = 0 \text{ and } \frac{\partial E^*_{tot}}{\partial y_i} = 0\ . \tag{A.6}$$

The derivatives $\frac{\partial E_{\mathrm{ext}}}{\partial x_i}$ and $\frac{\partial E_{\mathrm{ext}}}{\partial y_i}$ will correspond to the external forces $\mathbf{F}_{\mathrm{ext}}(\mathbf{v}_i) = (fx(x_i, y_i), fy(x_i, y_i))$.

[1)] Precautions have to be taken to avoid crossing over of contour nodes caused by the approximation of $\mathbf{v}_s$ and $\mathbf{v}_{ss}$. Regular normalization is required by interpolating the contour and re-distributing its nodes homogenously.

Optical Digital Image Processing. Fundamentals and Applications. Edited by

ISBN: xx-xxx-x-xxx-xxxxx-x

Hence for $\frac{\partial E^*_{tot}}{\partial x_i} = 0$ we obtain the following force component equation:

$$\begin{array}{l} w_1^i \frac{(x_i - x_{i-1})}{h^2} - w_1^{i+1} \frac{(x_{i+1} - x_i)}{h^2} + w_2^{i-1} \frac{(x_{i-2} - 2x_{i-1} + x_i)}{h^4} - \\ -2w_2^i \frac{(x_{i-1} - 2x_i + x_{i+1})}{h^4} + w_2^{i+1} \frac{(x_i - 2x_{i+1} + x_{i+2})}{h^4} = fx(x_i, y_i) \end{array} \tag{A.7}$$

or

$$\begin{array}{l} \frac{w_2^{i-1}}{h^4} x_{i-2} + x_{i-1}(-2\frac{w_2^{i-1}}{h^4} - 2\frac{w_2^i}{h^4} - \frac{w_1^i}{h^2}) + \\ x_i(\frac{w_2^{i-1}}{h^4} + 4\frac{w_2^i}{h^4} + \frac{w_2^{i+1}}{h^4} + \frac{w_1^i}{h^2} + \frac{w_1^{i+1}}{h^2}) + \\ x_{i+1}(-2\frac{w_2^i}{h^4} - 2\frac{w_2^{i+1}}{h^4} - \frac{w_1^{i+1}}{h^2}) + x_{i+2}\frac{w_2^{i+1}}{h^4} = fx(x_i, y_i) \, , \end{array} \tag{A.8}$$

or

$$c_{i-2}x_{i-2} + b_{i-1}x_{i-1} + a_i x_i + b_i x_{i+1} + c_i x_{i+2} = fx(x_i, y_i) \, . \tag{A.9}$$

Note that in the discrete formulation the energy related to stretch or tension gives rise to forces of the type $w_1^i \frac{(x_i - x_{i-1})}{h^2}$ which are analogue to kx in the mass-spring equation of (Eq. 1.26) given in Section 1.4.1. Hence, the discrete snake will behave partly - apart from the rigidity terms - like a closed set of connected springs.

For $\frac{\partial E^*_{tot}}{\partial y_i} = 0$ a similar equation can be found. In case we introduce a Nx2 matrix $\mathbf{V}$ with elements $\mathbf{v}_i = (x_i, y_i)$ and a Nx2 matrix $\mathbf{F}$ with elements $\mathbf{f}_i = (fx(x_i, y_i), fy(x_i, y_i))$, we can write the N equations in matrix form $\mathbf{AV} = \mathbf{F}$.

For a cyclic boundary condition like a closed contour we then obtain the following symmetric matrix:

$$\mathbf{A} = \begin{bmatrix} a_0 & b_0 & c_o & & & & c_{N-2} & b_{N-1} \\ b_0 & a_1 & b_1 & c_1 & & & & c_{n-1} \\ c_0 & b_1 & a_2 & b_2 & c_2 & & & \\ & c_1 & b_2 & a_3 & b_3 & c_3 & & \\ \ldots & \ldots & \ldots & \ldots & \ldots & \ldots & \ldots & \ldots \\ & & & c_{N-5} & b_{N-4} & a_{N-3} & b_{N-3} & c_{N-3} \\ c_{N-2} & & & & c_{N-4} & b_{N-3} & a_{N-2} & b_{N-2} \\ b_{N-1} & c_{N-1} & & & & c_{N-3} & b_{N-2} & a_{N-1} \end{bmatrix} \tag{A.10}$$

The dynamic formulations now become:

$$\begin{array}{l} \mathbf{A}\mathbf{x}(t) - \mathbf{f}\mathbf{x}(\mathbf{x}(t), \mathbf{y}(t)) = -\gamma \frac{\partial \mathbf{x}(t)}{\partial t} \\ \mathbf{A}\mathbf{y}(t) - \mathbf{f}\mathbf{y}(\mathbf{x}(t), \mathbf{y}(t)) = -\gamma \frac{\partial \mathbf{y}(t)}{\partial t} \, . \end{array} \tag{A.11}$$

Discretization in time leads to:

$$\begin{array}{l} \mathbf{A}\mathbf{x}_t - \mathbf{f}\mathbf{x}(\mathbf{x}_t, \mathbf{y}_t) = -\gamma(\mathbf{x}_t - \mathbf{x}_{t-1}) \\ \mathbf{A}\mathbf{y}_t - \mathbf{f}\mathbf{y}(\mathbf{x}_t, \mathbf{y}_t) = -\gamma(\mathbf{y}_t - \mathbf{y}_{t-1}) \, . \end{array} \tag{A.12}$$

As the forces in the new (unknown) positions $\mathbf{x}_t, \mathbf{y}_t$ are unknown themselves, a non-linear approach needs to be followed to solve the equations. Methods following such kind of approach are called implicit Euler methods and can in general use a large time-step. In case the forces are defined in terms of the current positions $\mathbf{x}_{t-1}, \mathbf{y}_{t-1}$,

they are known, and the equations become linear. Such an approach is called an explicit Euler method and is only valid if the differences in position or the time-step are kept small. Hence more iterations are needed, but solving the linear equations is much simpler and faster.

In the same way we could make $\mathbf{A}$ depending on the tension and rigidity parameters $w_1^{i,t-1} = w_1(x_{i,t-1}, y_{i,t-1})$ and $w_2^{i,t-1} = w_2(x_{i,t-1}, y_{i,t-1})$ of the previous time-step in case these parameters are time-dependent as well, giving rise to $\mathbf{A}_{t-1}$. Hence we obtain:

$$\mathbf{A}_{t-1}\mathbf{x}_t - \mathbf{fx}(\mathbf{x}_{t-1}, \mathbf{y}_{t-1}) = -\gamma(\mathbf{x}_t - \mathbf{x}_{t-1}) \; . \tag{A.13}$$

Regrouping of terms, considering $\mathbf{A}$ to be time independent, leads to:

$$[\mathbf{A} + \gamma\mathbf{I}]\mathbf{x}_t - \mathbf{fx}(\mathbf{x}_{t-1}, \mathbf{y}_{t-1}) - \gamma\mathbf{x}_{t-1} = 0 \; . \tag{A.14}$$

Solving for $\mathbf{x}_t$ results in:

$$\mathbf{x}_t = [\mathbf{A} + \gamma\mathbf{I}]^{-1}[\gamma\mathbf{x}_{t-1} + \mathbf{fx}(\mathbf{x}_{t-1}, \mathbf{y}_{t-1})] \; . \tag{A.15}$$

In a similar way we obtain also the solution for $\mathbf{y}_t$:

$$\mathbf{y}_t = [\mathbf{A} + \gamma\mathbf{I}]^{-1}[\gamma\mathbf{y}_{t-1} + \mathbf{fy}(\mathbf{x}_{t-1}, \mathbf{y}_{t-1})] \; . \tag{A.16}$$

The matrix $\mathbf{A} + \gamma\mathbf{I}$ is a pentadiagonal banded matrix, where γ is the step size. Coordinates $\mathbf{x}_t$ and $\mathbf{y}_t$ represent the solution to the equation of the snake, in case they no longer vary.

B
Model-based Segmentation: Examples

B.1
Model-based approach for the automatic extraction of linear features, like roads and paths, from aerial images [1]

Step1: Generation of an appropriate problem specific data structure The first step utilises local information related to the geometry and radiometry of the structures to be extracted. It consists of a series of morphological filtering stages, followed by a line-tracking algorithm, which produces a set of line segments (Fig. B.1b).

Step 2: Statistical labelling process (MAP-MRF) A segment linking process is carried out incorporating contextual, *a priori* knowledge about the road shape, with the use of MRF theory. The extracted line segments, produced by the morphological operators, are organised as a graph. The linking of these segments is then achieved through assigning labels to the nodes of the graph, using domain knowledge, extracted line segment measurements and spatial relationships between the various line segments. The interpretation labels are modelled as an MRF on the corresponding graph and the linear feature identification problem is formulated as a MAP estimation rule (Fig. B.1c).

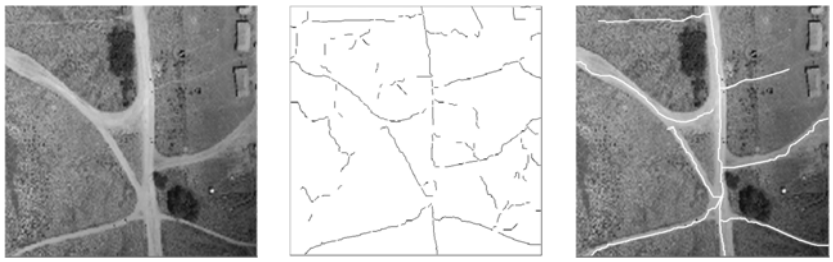

(a) (b) (c)

Fig. B.1 (a) Original image, (b) line segments and (c) final result, extraction of linear features

Optical Digital Image Processing. Fundamentals and Applications. Edited by

ISBN: xx-xxx-x-xxx-xxxxx-x

B.2
Sulci detection in cortical brain maps [2]

Step1: Generation of an appropriate problem specific data structure The cortical brain surface extracted from 3D MRI is unwrapped into a 2D plane [3]. The main tracks of the major sulci are split into line segments by an extraction algorithm originally implemented for road detection [1]. These line segments are considered as the building blocks for the approximation of the sulci. The sites correspond to these line segments and the anatomical class indices of the sulci are the labels.

Step 2: Statistical labelling process (MAP-MRF) The Markov Random Field (MRF) model proved already previously its usefulness for the analysis of classical MRI images of the brain [4]. In the labelling problem, described in [2], two types of cliques are defined: (1) first order cliques including one site, i.e. a single line segment and second order cliques C_2 involving two neighbouring line segments. The global minimum of the energy $U(\mathbf{r}|\mathbf{x})$ is determined by means of the stochastic Simulated Annealing (SA) algorithm [5]. The following observed features $\mathbf{x}_m$ are taken into consideration: the position (u_m, v_m) of the middle point of the line segment or site s_m, its orientation θ_m and its grey value g_m (which in our data representation is related to the depth of the Sulcus segment with respect to the 3D surface of the brain). The probabilities and probability densities:

$$P(r_m), P(r_m, r_{m'}) \text{ and } \mathrm{p}(\mathbf{x}_m|r_m) = p((u_m, v_m, \theta_m, g_m)|r_m)$$

and their related potentials:

$$\begin{aligned} V(r_m) &\propto - \ln(P(r_m)); \\ V(r_m, r_{m'}) &\propto - \ln(P(r_m, r_{m'})) \\ V(\mathbf{x}_m|r_m) &\propto - \ln(p(\mathbf{x}_m|r_m)) \end{aligned}$$

are estimated from the training set. As the order or indices of the sites in this particular problem are unknown a priori (the number and position of the line segments vary from one brain map to another) and due to the limited number of labeled maps (9 in total), it was assumed that all sites or couple of sites could be treated in the same way and were following the same statistical distribution. Hence:

$$\begin{aligned} &P(r_m = l_i) = P(r_{m'} = l_i), \\ &, \forall m \in \{1, \ldots, \mathrm{M}\}, \forall m' \in \{1, \ldots, \mathrm{M}\}; \\ &P(r_m = l_i, r_{m'} = l_j) = P(r_\mu = l_i, r_{\mu'} = l_j) \\ &, \forall m \in \{1, \ldots, \mathrm{M}\}, \forall m' \in \mathbf{N}(s_m), \\ &, \forall \mu \in \{1, \ldots, \mathrm{M}\}, \forall \mu' \in \mathbf{N}(s_\mu); \\ &P(\mathbf{x}_\mu|r_m = l_i) = P(\mathbf{x}_\mu|r_{m'} = l_i), \\ &\forall m \in \{1, \ldots, \mathrm{M}\}, \forall m' \in \{1, \ldots, \mathrm{M}\} \\ &, \text{ and this for any feature vector } \mathbf{x}_\mu. \end{aligned}$$

In the first experiments $p(\mathbf{x}_m|r_m)$ was modeled as the product of independent Gaussian distributions. Yet as the distribution of the positional features (u_m, v_m) of the sulci strongly deviates from a Gaussian distribution, we opted for an approach based on the Parzen window technique [6]. The Parzen window technique provides a non-parametric tool for density estimation.

In order to make this approach useful for teaching applications, the described algorithm has been integrated in a graphical user interface [2].

B.3
Identification of building rooftops based on MRF modeling [7]

Identification of building rooftops from a single remote sensing image based on 2D and 3D contextual information of the imaged scene has been described in [7]. The principles of perceptual organization are used for grouping line segments and contours, resulting in building rooftop hypotheses. An MRF model describes the dependencies between all available hypotheses with respect to global consistence.

B.4
A generic land cover classification method for vector-valued images [8]

A generic land cover classification method for vector-valued images has been described in [8]. Step 1 of the method generates a hierarchical data structure (MRAT, multiscale region adjacency tree) based on the deep image structure of the image data [9]. Step 2 is again based on the Bayesian-Markovian framework.

B.5
Model-based measurement of skin thickness in mammography based on MRF-MAP

Model-based measurement of skin thickness in mammography based on MRF-MAP. As usual, the first step generates an appropriate problem specific data structure. In this case we chose the multi-scale gray level gradient estimation, using a wavelet decomposition of the image. Subsequently, the spatial distribution of this feature is organized as a graph, with each of its nodes associated with a binary set of labels (skin/no_skin). For the identification of the region of the skin, we define a neighborhood system and an MRF on the binary set of labels. The labeling problem is then formulated as a MAP estimation rule [10, 11].

References

1 Katartzis, A. et al., "A model-based approach to the automatic extraction of linear features from airborne images," *IEEE Transactions on Geoscience and Remote Sensing*, 39, pp. 2073–2079, 2001.

2 Deklerck, R., Suliga, M. and Nyssen, E., "An intelligent tool to aid in understanding cortical brain anatomy visualized by means of flat maps," in "Proceedings of the 3rd IASTED International Conference on Web-Based Education," pp. 474–479, 2004.

3 Deklerck, R. et al., "A method to construct flat maps of the brain's surface and its application," *International Journal of Pattern Recognition and Artificial Intellegence*, 20, pp. 679–709, 2006.

4 Riviere, D. et al., "Relational graph labelling using learning techniques and markov random fields," *16th International Conference on Pattern Recognition*, 2, p. 20172, 2002.

5 Geman, S. and Geman, D., "Stochastic relaxation, gibbs distributions and the bayesian restoration of images," *IEEE Transactions on Pattern Analysis and Machine Intelligence*, 6, pp. 721–741, 1984.

6 Duda, R. O. and Hart, P. E., *Pattern Classification and Scene Analysis*, John Wiley & Sons, Inc., 1973.

7 Katartzis, A. and Sahli, H., "A stochastic framework for the identification of building rooftops using a single remote sensing image," *IEEE Transactions on Geoscience and Remote Sensing*, 46, pp. 259–271, 2008.

8 Katartzis, A., Vanhamel, I. and Sahli, H., "A hierarchical markovian model for multiscaleregion-based classification of vector valued images," *IEEE Transactions on Geoscience and Remote Sensing*, 43, pp. 548–558, 2005.

9 Koenderink, J. J., "The structure of images," *Biological Cybernetics*, 50, pp. 363–370, 1984.

10 Katartzis, A. et al., "Model-based technique for the measurement of skin thickness in mammography," *Medical and Biological Engineering and Computing*, 40, pp. 153–162, 2002.

11 Katartzis, A. et al., *Medical Image Analysis Methods*, chapter A MRF-based approach for the measurement of skin thickness in mammography, pp. 315–340, CRC Taylor and Francis Group, 2005.

Optical Digital Image Processing. Fundamentals and Applications. Edited by

ISBN: xx-xxx-x-xxx-xxxxx-x